

Article

Influence of Reduction Temperature on the Structure and Naphthalene Hydrogenation Saturation Performance of Ni₂P/Al₂O₃ Catalysts

Ze Li ^{1,2}, Jie-Ying Jing ^{1,2,*} , Zhi-Qiang Qie ^{1,2} and Wen-Ying Li ^{1,2} 

¹ State Key Laboratory of Clean and Efficient Coal Utilization, Taiyuan University of Technology, Taiyuan 030024, China; lize0838@link.tyut.edu.cn (Z.L.); qiezhiquang0532@link.tyut.edu.cn (Z.-Q.Q.); ying@tyut.edu.cn (W.-Y.L.)

² Key Laboratory of Coal Science and Technology, Taiyuan University of Technology, Ministry of Education, Taiyuan 030024, China

* Correspondence: jingjieying@tyut.edu.cn

Abstract: Jet fuel rich in hydroaromatics and cycloalkanes could be derived from direct coal liquefaction oil via the hydrogenation saturation process. Developing an efficient catalyst to transform naphthalene hydrocarbons to hydroaromatics and cycloalkanes with high selectivity plays a significant role in realizing the above hydrogenation saturation process. In this work, Ni₂P/Al₂O₃ catalysts were prepared at different reduction temperatures via the thermal decomposition of hypophosphite. We investigated the influence of reduction temperature and the results showed that reduction temperature had an important impact on the properties of Ni₂P/Al₂O₃ catalysts. When the reduction temperature was 400 °C, the Ni₂P particle size of the Ni₂P/Al₂O₃ catalyst was 3.8 nm and its specific surface area was 170 m²/g. Furthermore, the Ni₂P/Al₂O₃ catalyst reduced at 400 °C obtained 98% naphthalene conversion and 98% decalin selectivity. The superior catalytic activity was attributed to the smaller Ni₂P particle size, higher specific surface area and suitable acidity, which enhanced the adsorption of naphthalene on Ni₂P/Al₂O₃ catalyst.

Keywords: nickel phosphide; reduction temperature; naphthalene hydrogenation; thermal decomposition of hypophosphite



Citation: Li, Z.; Jing, J.-Y.; Qie, Z.-Q.; Li, W.-Y. Influence of Reduction Temperature on the Structure and Naphthalene Hydrogenation Saturation Performance of Ni₂P/Al₂O₃ Catalysts. *Crystals* **2022**, *12*, 318. <https://doi.org/10.3390/cryst12030318>

Academic Editors: Felix Jaetae Seo, William Yu and Sanju Gupta

Received: 20 January 2022

Accepted: 23 February 2022

Published: 24 February 2022

Publisher's Note: MDPI stays neutral with regard to jurisdictional claims in published maps and institutional affiliations.



Copyright: © 2022 by the authors. Licensee MDPI, Basel, Switzerland. This article is an open access article distributed under the terms and conditions of the Creative Commons Attribution (CC BY) license (<https://creativecommons.org/licenses/by/4.0/>).

1. Introduction

The process of transforming direct coal liquefaction oil into high performance jet fuel has notable features such as low hydrogen consumption, the high added value of the product, and it conforms to our national requirements [1–3]. The main point of the whole process is the preparation of efficient hydrogenation catalysts for aromatics' hydrogenation saturation in the feedstock. Naphthalene is a typical aromatic ring compound contained in direct coal liquefaction oil; nevertheless, it is very difficult to realize complete saturation in the hydrogenation process [4]. The traditional transition metal sulfide hydrogenation catalysts perform poorly in the naphthalene hydrogenation process [5,6], and the required reaction conditions are generally harsh, which makes it difficult to meet the actual production requirements. Although the noble metal catalysts have good hydrogenation activity [7,8], their low yield and high price are not conducive to large-scale industrial applications. Thus, the development of efficient and easily available hydrogenation catalysts has become urgent in order to realize the process of transforming direct coal liquefaction oil into high-performance jet fuel.

In recent years, Ni₂P catalysts have shown high intrinsic hydrogenation activity in hydrodesulfurization [9,10] and hydrodenitrogenation reactions [11,12] due to their special crystal morphology and physicochemical properties, and they are expected to be the new generation of highly efficient aromatic hydrosaturation catalysts [13,14]. Unlike metal

carbides and nitrides, the radius of P atoms (0.109 nm) is much larger than that of C atoms (0.071 nm) and N atoms (0.065 nm). In order to stabilize the crystal structure, P atoms cannot enter the metal lattice interstices, but can only enter the trigonal structure of the phosphide and occupy its internal voids, forming a filled compound. Compared with the layered structure of commercial metal sulfide catalysts, the spherical structure of transition metal phosphide catalysts, which consists of stacked trigonal structural units, has more prismatic and angular positions, which can provide more ligand-unsaturated surface atoms and expose more active sites for hydrogenation reactions.

It has been proven that Ni₂P has the highest catalytic activity among many phosphide catalysts and Ni₂P catalysts have been applied to aromatic hydrogenation reactions [15–20]. Weber et al. found that the higher the dispersion of Ni₂P, the better the hydrodesulfurization performance of the catalyst [21]. Oyama et al. found that the smaller the Ni₂P particles, the stronger the Ni-P bond in the Ni₂P active phase formed, which could enhance the activity and stability of the catalyst [22]. Li and Ni et al. found that the phase composition and morphology of Ni₂P were closely related to its hydrodesulfurization and hydrodenitrogenation reaction activity [23,24].

Al₂O₃ is commonly used as a carrier for hydrogenation catalysts in industry, however, when Ni₂P/Al₂O₃ was prepared by the traditional programmed-temperature reduction method, it was difficult to prepare the Ni₂P active phase on Al₂O₃ carrier, which was due to the strong interaction between Al₂O₃ and P species in the precursor to form AlPO₄ at high roasting temperatures; this seriously limits the application of Al₂O₃ carrier in Ni₂P catalysts [25–28]. It is generally believed that the interaction between Al₂O₃ and P becomes weaker at low temperatures, and researchers have successfully prepared Ni₂P catalysts by thermal decomposition of hypophosphite at low temperatures. It has been shown that the preparation of Ni₂P catalysts by the thermal decomposition of hypophosphite is strongly influenced by the reduction temperature. At lower reduction temperatures, the generated Ni₂P phase is impure and less abundant, while at higher reduction temperatures, the dispersion of the Ni₂P phase decreased and aggregated to form large Ni₂P particles, which reduced the catalyst activity. Lan et al. obtained Ni₂P/SiO₂ catalysts by reducing the catalyst precursors at 350 °C, 450 °C and 550 °C using phosphite and hypophosphite as phosphorus source, respectively. They found that the catalysts prepared at 450 °C had the optimal hydrodeoxygenation performance, which was related to their higher number of active sites and higher dispersion [21]. Therefore, in the preparation of Ni₂P catalysts by the thermal decomposition of hypophosphite, the reduction temperature not only affects the morphology, particle size, dispersion, and reduction degree of the Ni₂P active phase, but also affects the catalyst surface properties, which in turn affects the catalyst activity. However, most of the current studies have investigated the effect of reduction temperature on the catalyst structure in inert carriers (SiO₂, MCM-41). We know that even for the same active components, different supports can lead to different catalyst microstructures of the active components, which in turn affect the hydrogenation saturation performance of the catalysts.

Therefore, the Ni₂P/Al₂O₃ catalyst was prepared by thermal decomposition using the hypophosphite method, and the influence of the reduction temperature on the Ni₂P phase formation, Ni₂P crystal structure, Ni₂P particle size and its naphthalene hydrogenation saturation performance was investigated.

2. Materials and Methods

The isovolumetric impregnation method was employed to synthesize the catalysts as described in our previous work [18], and Ni loading was kept at 10 wt.%. Firstly, a certain amount of nickel acetate tetrahydrate (Ni(CH₃COO)₂·4H₂O, analytical pure, Tianjin Kemiou Chemical Reagent Co., Ltd., Tianjin, China) and ammonium hypophosphite (NH₄H₂PO₂, analytical pure, Aladdin, Shanghai, China) were dissolved in the proper amount of distilled water according to the P/Ni molar ratio of 2 to obtain a uniform solution. Then a certain amount of Al₂O₃ powder (99.99%, Aladdin, Shanghai, China) was

slowly added to the obtained solution and stirred at room temperature for 12 h, and the catalyst precursor was obtained after being dried at 60 °C for 12 h. The precursor was reduced in an H₂ atmosphere at a rate of 2 °C min⁻¹ at different reduction temperatures and maintained for 2 h with a H₂ flow rate of 100 mL min⁻¹. To prevent the oxidation of the catalyst by vapor and oxygen in the air, the reduction procedure was ended by passivation with 1% vol of O₂/N₂ at a gas flow rate of 30 mL min⁻¹ for 1 h. The catalysts were marked as Cat-300, Cat-350, Cat-400, Cat-450, Cat-500 according to the differences in the reduction temperature. Furthermore, PH₃ might be produced during the precursor decomposition process; thus, the generated PH₃ was recovered according to the following reaction principle, which is shown in Equation (1).



An X-ray diffractometer (Rigaku, Japan) was used to analyze the crystal structure of the catalysts. The Cu target was employed as the radiation source, the tube voltage and tube current were 40 kV and 40 mA, respectively, the scanning angle was 10–80° and the scanning rate was 8° min⁻¹. The specific surface area and pore structure tests of the catalysts were performed using a JW-BK122W physical adsorption instrument. The catalysts were pretreated in a vacuum atmosphere at 300 °C for 3 h. The N₂ adsorption–desorption experiments were done at –196 °C, and the specific surface area of the catalysts was calculated by the BET equation. The morphology of catalysts was observed via transmission electron microscope (JEM-2100F, Japan Co., Ltd., Tokyo, Japan). The surface elemental state of the catalysts was analyzed by X-ray photoelectron spectrometer (ESCALAB 250Xi, Thermo Fisher Scientific, Waltham, MA, USA). The CO pulse adsorption experiments were carried out to monitor the active site number of catalysts on AutochemII 2920 Chemisorption Analyzer (Micromeritics, Atlanta, GA, USA). First, 100 mg catalyst was put in a U-shaped quartz tube, and reduced at 360 °C for 2 h in 10 vol% H₂/Ar flow with a rate of 50 mL min⁻¹. After the reduction, the temperature was decreased to room temperature under Ar gas, and then 5 vol% CO/Ar was pulsed into the reactor with 0.1 mL sampling loop capacity until the adsorption saturation. NH₃-TPD analysis was performed on an AutochemII 2920 Chemisorption Analyzer (Micromeritics, Atlanta, GA, USA) to analyze the acidic properties of the catalysts. A total of 0.06 g of passivated catalyst was first reduced by 10 vol% H₂/Ar gas with a flow rate of 50 mL min⁻¹ for 2 h at a certain temperature, which was 40 °C lower than the corresponding reduction temperature. After reduction, the catalysts were cooled to 100 °C in a He atmosphere, and then the gas was switched to 3 vol% NH₃/He mixture to adsorb NH₃ at 100 °C for 30 min. The temperature was then increased to 700 °C at a rate of 10 °C min⁻¹ for NH₃ desorption in a He atmosphere. Pyridine infrared adsorption (Py-IR) was used to analyze the acidity type and the acidity values via Fourier transform infrared spectrometer (Tensor 27, Bruker, Baden-Württemberg Karlsruhe, Germany). Then, 0.01 g catalyst was evaluated in situ at 400 °C for 1 h under vacuum (10⁻² Pa), and cooled down to room temperature to record the sample skeleton. Pyridine was introduced for adsorption. After removing the excess pyridine in the tube, the temperature was increased to 150 °C and kept for 1 h. The pyridine infrared spectrum was obtained when the temperature was dropped to room temperature.

Next, 0.2 g of the catalysts (0.25–0.42 mm) was placed in the reaction tube of a fixed-bed reactor to evaluate the naphthalene hydrogenation performance. The catalyst was first reduced at different reduction temperatures in the presence of 100 mL min⁻¹ H₂ for 2 h, and then 3 wt.% naphthalene in decane was fed at a rate of 6 mL h⁻¹ and H₂ was fed at a rate of 60 mL min⁻¹. The reaction temperature was 300 °C, and the reaction pressure was 4.0 MPa. Each hydrogenation saturation reaction proceeded for 8 h. Every hour we sampled the hydrogenation saturation products and they were analyzed by GC after mixing them with dodecane. All the reactions were carried out 3 times, and the recorded data were thought to

be accurate when the relative deviation was less than 3%. The following formula presents the method used to evaluate the hydrogenation saturation performance.

$$X_{C_{10}H_8} = \frac{N_{C_{10}H_8,in} - N_{C_{10}H_8,out}}{N_{C_{10}H_8,in}} \times 100\% \quad (2)$$

$$S_j = \frac{N_j}{\sum N_j} \times 100\% \quad (3)$$

Herein, $X_{C_{10}H_8}$ is naphthalene conversion, S_j is product selectivity, $N_{C_{10}H_8,out}$ is the amount of inlet $C_{10}H_8$, mol, $N_{C_{10}H_8,in}$ is the amount of outlet $C_{10}H_8$, mol, N_j is the amount of each product, mol, and $\sum N_j$ is the total amount of all products, mol.

3. Results

3.1. Characterization of the Catalysts

3.1.1. Crystalline Structure

Figure 1 shows the XRD patterns of different Ni_2P/Al_2O_3 catalysts. As shown in Figure 1, when the reduction temperature was 300–400 °C, the prepared catalysts only showed diffraction peaks at 45.59° and 67.37°, which belong to the Al_2O_3 (PDF: 29-0063) support, and no characteristic diffraction peaks of Ni_2P appeared. This might be due to the low content of the generated Ni_2P or the highly dispersed state of Ni_2P [19]. When the reduction temperature increased to 450 °C, the catalyst started to show the characteristic diffraction peaks of Ni_2P at 40.7° and 54.2° (PDF:03-0953). When the reduction temperature was further elevated to 500 °C, compared to the catalyst reduced at 450 °C, the intensity of the diffraction peaks became stronger and the half-peak width became narrower, which indicated that the grain size of Ni_2P gradually became larger as the reduction temperature increased. Comparing the diffraction peak patterns of the catalysts prepared at different reduction temperatures, it can be seen that the grain size of Ni_2P gradually increased with the increase in the reduction temperature, indicating that Ni_2P was continuously reduced out during the process.

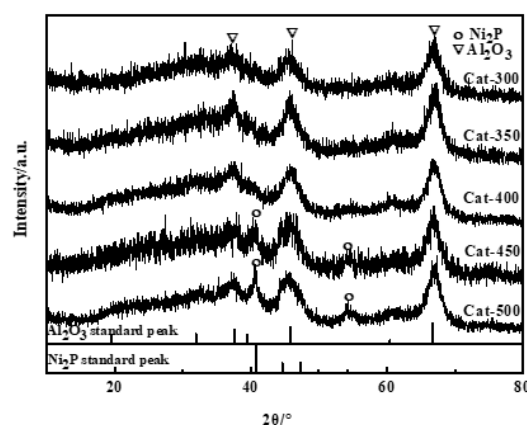


Figure 1. X-ray diffraction spectra of different Ni_2P/Al_2O_3 catalysts.

3.1.2. Morphology and Particle Size

The morphology of different Ni_2P/Al_2O_3 catalysts are shown in Figure 2. It was found that the morphology of Ni_2P catalysts was spherical, and this was beneficial as it led to better dispersion on Al_2O_3 and exposed more active sites, resulting in higher hydrogenation activity [20]. When the reduction temperature was 300–400 °C, the Ni_2P particles were uniformly and highly dispersed on the Al_2O_3 support, while partial agglomeration of the Ni_2P particles occurred when the reduction temperatures increased to 450 °C and 500 °C. The particle sizes of the Ni_2P/Al_2O_3 catalysts prepared at different reduction temperatures are listed in Table 1. The results showed that the particle size gradually increased with the

increase in the reduction temperature (3 nm \rightarrow 7 nm), and this trend was consistent with the XRD results. It was noteworthy that the particle size growth rate of the reduced $\text{Ni}_2\text{P}/\text{Al}_2\text{O}_3$ catalysts was slow when the reduction temperature was less than 400 $^\circ\text{C}$, however, when the reduction temperature was higher than 400 $^\circ\text{C}$, the particle size growth rate of the reduced $\text{Ni}_2\text{P}/\text{Al}_2\text{O}_3$ catalysts was faster, which was due to the agglomeration in the catalysts prepared at 450 $^\circ\text{C}$ and 500 $^\circ\text{C}$, resulting in larger Ni_2P particles. High-resolution TEM images of $\text{Ni}_2\text{P}/\text{Al}_2\text{O}_3$ catalysts prepared at different reduction temperatures further demonstrated that the lattice spacing of all the prepared catalysts was 0.22 nm, which was consistent with the crystallographic spacing of the Ni_2P (111), indicating that the Ni_2P active phase could be generated when the reduction temperature was between 300–500 $^\circ\text{C}$.

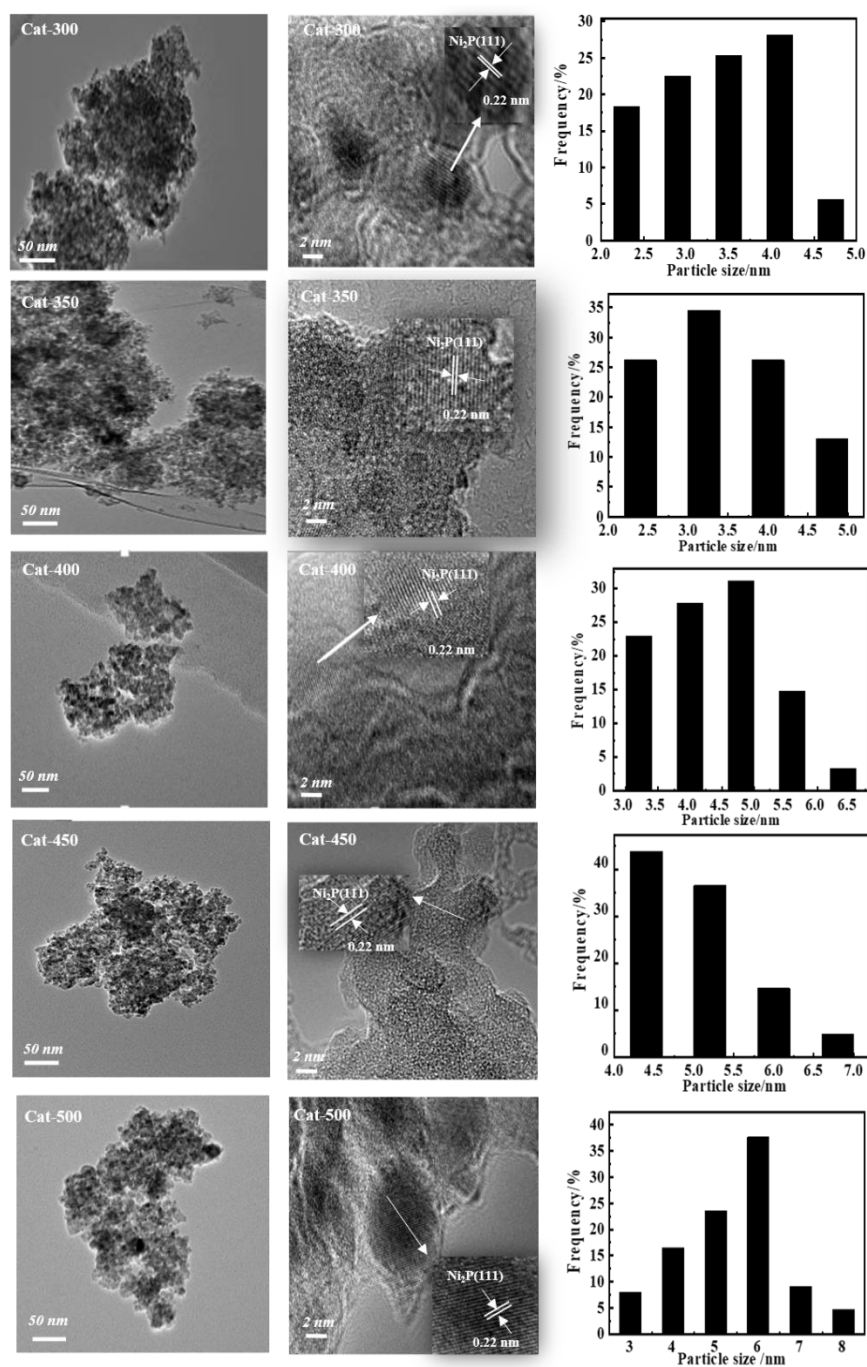


Figure 2. TEM micrographs of different $\text{Ni}_2\text{P}/\text{Al}_2\text{O}_3$ catalysts.

Table 1. $\text{Ni}^{\delta+}$ and $\text{P}^{\delta-}$ peak area of different $\text{Ni}_2\text{P}/\text{Al}_2\text{O}_3$ catalysts.

Catalyst	$\text{Ni}^{\delta+}$ Peak Area	$\text{P}^{\delta-}$ Peak Area	$\text{Ni}^{\delta+}$ area Percentage (%)	$\text{P}^{\delta-}$ Area Percentage (%)
Cat-300	6053	214	9.95	11.29
Cat-350	7256	507	11.67	18.40
Cat-400	9506	519	32.91	28.66
Cat-450	3735	257	15.72	12.47
Cat-500	2450	209	11.03	12.67

3.1.3. Electronic Properties

In order to investigate the surface composition and elemental valence of the catalysts, the $\text{Ni}_2\text{P}/\text{Al}_2\text{O}_3$ catalysts prepared at different reduction temperatures were characterized by XPS. Figure 3 presents the XPS spectra of Ni 2p and P 2p on $\text{Ni}_2\text{P}/\text{Al}_2\text{O}_3$ catalysts prepared at different reduction temperatures. According to the literature [21,22], the 2p electron orbital decomposition of the Ni atom splits into $\text{Ni } 2p_{1/2}$ and $\text{Ni } 2p_{3/2}$, and each has a companion peak. The binding energies between 853.0 and 853.5 eV were caused by $\text{Ni}^{\delta+}$, and the binding energies between 856.0 and 857.3 eV were caused by Ni^{2+} interacting with PO_4^{3-} . It is generally believed that the binding energy in the range of 129.0–129.5 eV was due to $\text{P}^{\delta-}$, 133.0–133.7 eV binding energy was due to the unreduced HPO_4^{2-} , and the binding energy at 134–135 eV was due to PO_4^{3-} derived from surface passivation. From Figure 3a, it can be seen that $\text{Ni}^{\delta+}$ ($0 < \delta < 1$) and Ni^{2+} were present on all the catalysts; and combined with the high-resolution TEM results in Figure 2, it is clear that $\text{Ni}_2\text{P}/\text{Al}_2\text{O}_3$ catalysts can be prepared by reducing the precursors at 300–500 °C. Comparing the peak patterns of catalysts prepared at different reduction temperatures, it was seen that the $\text{Ni}^{\delta+}$ area percentage (Table 1) became larger with the increased reduction temperature when the $\text{Ni}_2\text{P}/\text{Al}_2\text{O}_3$ catalysts were prepared at reduction temperatures of 300–400 °C, which indicated that $\text{Ni}^{\delta+}$ was continuously reduced out with the increase in reduction temperature. When the reduction temperature was higher than 400 °C, the $\text{Ni}^{\delta+}$ area percentage became smaller with the further increase in the reduction temperature, which suggested that the catalysts prepared at 400 °C possessed the most Ni_2P active phases. From Figure 3b, it can be seen that $\text{P}^{\delta-}$ ($0 < \delta < 1$) appeared on all the catalysts and the $\text{P}^{\delta-}$ area percentage increased gradually with the increasing reduction temperature. The Cat-400 catalyst had the largest $\text{P}^{\delta-}$ area percentage, indicating that Cat-400 had the most Ni_2P active phases. The peaks appearing at 133.7 eV and 134.2 eV for the Cat-300 catalyst were attributed to HPO_4^{2-} and PO_4^{3-} ; the former was due to the precursor decomposition while the latter was the result of a combination of the precursor decomposition and the passivation process. No H_2PO_2^- peak appeared, which indicated that the precursor could be decomposed completely at 300 °C, producing the unreduced HPO_4^{2-} and PO_4^{3-} . In contrast, when the reduction temperature was higher than 350 °C, only the peak of PO_4^{3-} was present in the catalyst, which indicated that HPO_4^{2-} was reduced completely at 350 °C.

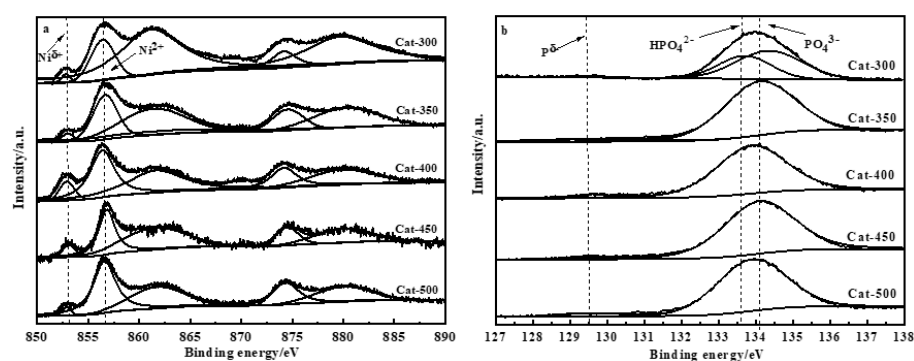


Figure 3. XPS patterns in the Ni 2p and P 2p regions of different $\text{Ni}_2\text{P}/\text{Al}_2\text{O}_3$ catalysts (a) Ni 2p (b) P 2p.

3.1.4. Acidic Analysis

The reduction temperature not only affected the Ni_2P active phase, but also had an important effect on the catalyst's surface acid content and strength, etc. Therefore, the different $\text{Ni}_2\text{P}/\text{Al}_2\text{O}_3$ catalysts were analyzed by NH_3 -TPD (Figure 4). As shown in Figure 4, compared with the blank Al_2O_3 support, $\text{Ni}_2\text{P}/\text{Al}_2\text{O}_3$ catalysts prepared at reduction temperatures of 300–400 °C showed a clear NH_3 desorption peak near 210 °C, meaning that there was weak acid in the catalyst, which was caused by the deposition of P-OH in the catalyst. According to the NH_3 -TPD principle, we know that the desorption peak area size was in direct proportion to the amount of acid on the catalyst surface. When the reduction temperature was elevated from 300 °C to 400 °C, the NH_3 desorption peak area decreased, suggesting that the acid content on the catalyst surface gradually decreased, which may be due to the increase in the reduction temperature, the P species on the catalyst surface were gradually reduced out, resulting in the decrease in the acid content. When the reduction temperature increased from 400 °C to 500 °C, the NH_3 desorption temperature decreased by about 30 °C (210 °C \rightarrow 180 °C), which implied that the intensity of the catalyst surface acid became lower as the reduction temperature increased when the reduction temperature was higher than 400 °C.

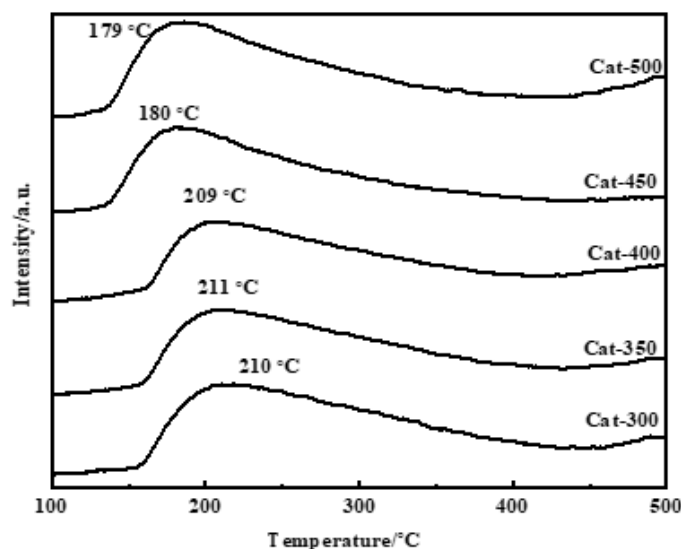


Figure 4. NH_3 -TPD profiles of different $\text{Ni}_2\text{P}/\text{Al}_2\text{O}_3$ catalysts.

In order to further understand the acidic type and the acidity values of different $\text{Ni}_2\text{P}/\text{Al}_2\text{O}_3$ catalysts, the catalysts were subjected to pyridine infrared adsorption (Py-IR, Table 2). From Table 2, it can be seen that the blank Al_2O_3 support only possessed Lewis acidity. When Ni_2P was formed on the Al_2O_3 , the acidic type and the acidity values of the $\text{Ni}_2\text{P}/\text{Al}_2\text{O}_3$ catalysts were changed. It was clear that the Lewis acidity value of all the $\text{Ni}_2\text{P}/\text{Al}_2\text{O}_3$ catalysts was much higher than that of the Bronsted acidity. When the reduction temperature increased from 300–400 °C, the Lewis acidity value gradually decreased, which was due to the fact that more Ni_2P particles were reduced and blocked the acid sites on the catalyst surface. When the reduction temperature was 400–500 °C, the Lewis acidity value decreased greatly. Combined with NH_3 -TPD analysis, this phenomenon might be due to the enhanced interaction between P species and the hydroxyl groups on Al_2O_3 .

3.1.5. Textural and Structural Property

In the preparation process of $\text{Ni}_2\text{P}/\text{Al}_2\text{O}_3$ catalysts, the reduction temperature not only affected the generation of Ni_2P , but also had an effect on the deposition of phosphorus on the catalyst surface, which in turn affected the specific surface area and pore structure

of the catalyst. Table 1 shows the specific surface area and pore structure parameters of different Ni₂P/Al₂O₃ catalysts. As shown in Table 3, the specific surface area and pore size of the catalysts varied with the reduction temperatures. It is noteworthy that the Cat-300 catalysts showed the smallest specific surface area and pore size, which might be due to the fact that after reducing the catalyst precursors at 300 °C, there were still a large amount of unreduced Ni species and P species in the catalysts, decreasing the specific surface area and pore size of the catalysts. The specific surface area and pore size of the catalysts tended to increase and then decrease with the increasing reduction temperature. The Cat-400 catalyst had the largest specific surface area and pore size. This was because the initial increase in the reduction temperature decreased the amount of P deposited on the catalyst surface and Ni₂P was continuously reduced out (see the XPS analysis in Figure 3). As the reduction temperature increased from 400 °C to 500 °C, the generated Ni₂P particles were prone to aggregate and the increased interaction between P and Al₂O₃ in the precursor led to a decrease in the specific surface area and pore size.

Table 2. Acidity values of different Ni₂P/Al₂O₃ catalysts.

Catalysts	Bronsted Acidity Value (μmol g ⁻¹)	Lewis Acidity Value (μmol g ⁻¹)
Cat-300	3.6	190.3
Cat-350	3.3	180.3
Cat-400	0.4	158.2
Cat-450	0.2	61.8
Cat-500	0.1	53.4
Al ₂ O ₃	0	131.8

Table 3. Textural and structural property of different Ni₂P/Al₂O₃ catalysts.

Catalyst	Specific Surface Area (m ² g ⁻¹)	Pore Size (nm)	Particle Size ^a (nm)	CO Uptake (μmol g ⁻¹)
Cat-300	134	2.8	3.2	13
Cat-350	163	3.8	3.4	19
Cat-400	170	5.2	3.8	30
Cat-450	159	4.3	5.1	22
Cat-500	158	3.4	7.2	17

^a: obtained from TEM results.

The active site number of different catalysts was evaluated via CO pulse adsorption and are presented in Table 1. It was clear that the CO uptake first increased and then decreased as the reduction temperature increased. For instance, the Cat-400 catalyst obtained the largest CO uptake, indicating that Cat-400 possessed the largest Ni₂P active sites on the surface of the catalyst. Combined with the analysis of BET, TEM (Figure 2) and NH₃-TPD (Figure 4), it is clear that when the reduction temperature increased from 300 °C to 400 °C, the generation of the reduced Ni₂P active phase increased, and the unreduced P species on the surface decreased, which exposed more active sites; correspondingly, the CO uptake increased whereas when the reduction temperature was further elevated to 450 °C or 500 °C, the CO uptake gradually declined. This could be ascribed to the Ni₂P agglomeration and P species deposition.

3.2. Naphthalene Hydrogenation Performance

The naphthalene hydrogenation saturation performance was evaluated for different Ni₂P/Al₂O₃ catalysts. The reaction was conducted at 300 °C, 4 MPa, and the reactants were 3 wt.% naphthalene in decane solution. From Figure 5, it is clear that hydrogenation activity of the Cat-400 catalyst was significantly better than other catalysts, with the catalytic activity of Cat-400 > Cat-450 > Cat-350 > Cat-300 > Cat-500. After reacting for 8 h, the conversion of naphthalene over the Cat-400 catalyst was 98%, and the decalin selectivity was 98%.

Combined with the XRD, BET and TEM characterization results, it can be seen that nickel and phosphorus in the Cat-400 catalyst precursor can be fully reduced to small particles of Ni_2P active phase with high dispersion, and more active sites were exposed on the catalyst surface, which determined the highest CO adsorption value ($30 \mu\text{mol g}^{-1}$, Table 1). In contrast, although the naphthalene conversion reached 95% on Cat-300 and Cat-350 catalysts, the product was dominated by the partially hydrogenated product, tetralin. This was mainly due to the fact that the nickel and phosphorus in the precursors of the Cat-300 and Cat-350 catalysts were not fully reduced to the Ni_2P active phase and contained a large amount of unreduced P species, which covered the active sites of $\text{Ni}_2\text{P}/\text{Al}_2\text{O}_3$ catalysts at the lower reduction temperature. Their CO adsorption value was 13 and $19 \mu\text{mol g}^{-1}$, respectively, which resulted in low hydrogenation selectivity. Compared with the Cat-400 catalyst, the catalytic activity of the Cat-450 and Cat-500 catalysts decreased, especially the product on Cat-500 catalyst, which was already dominated by tetralin, indicating that the higher reduction temperature had a detrimental effect on the catalyst activity. When the reduction temperature was higher, the particle size of the Ni_2P active phase increased, which leads to a decrease in the number of active sites (Table 1), and on the other hand, the strong interaction of P species in the precursor with Al_2O_3 during the reduction process would cause a large decrease in the acid strength of the catalyst.

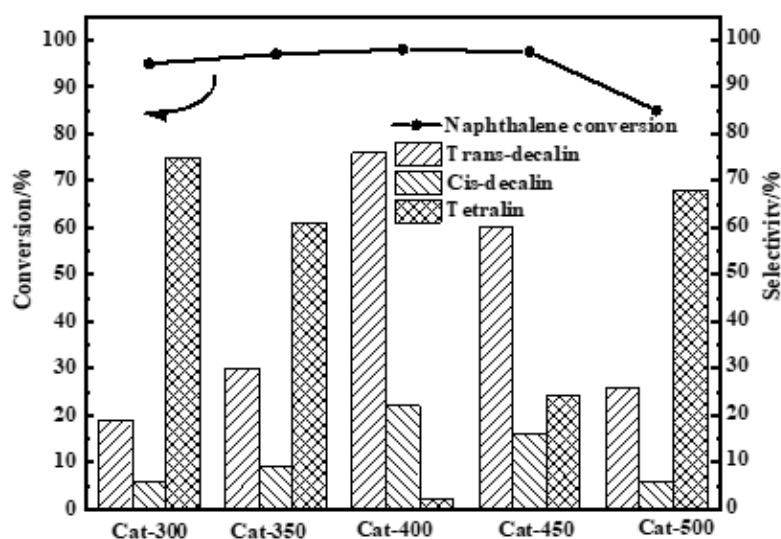


Figure 5. Catalytic activity of different $\text{Ni}_2\text{P}/\text{Al}_2\text{O}_3$ catalysts.

4. Conclusions

$\text{Ni}_2\text{P}/\text{Al}_2\text{O}_3$ catalysts were synthesized at different reduction temperature. The specific surface area, particle size, active sites and the surface acidity were tuned by changing the reduction temperature. Naphthalene hydrogenation saturation evaluation showed that Cat-400 displayed a 98% naphthalene conversion and 98% decalin selectivity at $300 \text{ }^\circ\text{C}$, 4 MPa. It was concluded that the large specific surface area, small particle size, more active sites and the suitable acidity contributed to the improved catalytic activity.

Author Contributions: Conceptualization, J.-Y.J.; data curation, Z.L. and Z.-Q.Q.; writing—original draft preparation, Z.L.; writing—review and editing, J.-Y.J. and W.-Y.L.; supervision, J.-Y.J.; project administration, J.-Y.J.; funding acquisition, J.-Y.J. and W.-Y.L. All authors have read and agreed to the published version of the manuscript.

Funding: This research was funded by the National Natural Science Foundation of China (21978190, 22038008).

Institutional Review Board Statement: Not applicable.

Informed Consent Statement: Not applicable.

Data Availability Statement: Not applicable.

Acknowledgments: Not applicable.

Conflicts of Interest: The authors declare no conflict of interest.

References

1. Yoon, E.M.; Selvaraj, L.; Song, C.; Stallman, J.B.; Coleman, M.M. High-temperature stabilizers for jet fuels and similar hydrocarbon mixtures. 1. Comparative studies of hydrogen donors. *Energy Fuel* **1996**, *10*, 806–811. [[CrossRef](#)]
2. Zhang, X.W.; Pan, L.; Wang, L.; Zou, J.J. Review on synthesis and properties of high-energy-density liquid fuels: Hydrocarbons, nanofluids and energetic ionic liquids. *Chem. Eng. Sci.* **2018**, *180*, 95–125. [[CrossRef](#)]
3. Jia, T.h.; Zhang, X.w.; Liu, Y.; Gong, S.; Deng, C.; Pan, L.; Zou, J.J. A comprehensive review of the thermal oxidation stability of jet fuels. *Chem. Eng. Sci.* **2021**, *229*, 116157. [[CrossRef](#)]
4. Beltramone, A.R.; Resasco, D.E.; Alvarez, W.E.; Choudhary, T.V. Simultaneous hydrogenation of multiring aromatic compounds over NiMo Catalyst. *Ind. Eng. Chem. Res.* **2008**, *47*, 7161–7166. [[CrossRef](#)]
5. Fu, W.Q.; Zhang, L.; Wu, D.F.; Xiang, M.; Zhuo, Q.; Huang, K.; Tao, Z.D.; Tang, T.D. Mesoporous zeolite-supported metal sulfide catalysts with high activities in the deep hydrogenation of phenanthrene. *J. Catal.* **2015**, *330*, 423–433. [[CrossRef](#)]
6. Badoga, S.; Dalai, A.K.; Adjaye, J.; Hu, Y. Combined effects of EDTA and heteroatoms (Ti, Zr, and Al) on catalytic activity of SBA-15 supported NiMo catalyst for hydrotreating of heavy gas oil. *Ind. Eng. Chem. Res.* **2014**, *53*, 2137–2156. [[CrossRef](#)]
7. Du, M.X.; Qin, Z.F.; Ge, H.; Li, X.K.; Lü, Z.J.; Wang, J.G. Enhancement of Pd–Pt/Al₂O₃ catalyst performance in naphthalene hydrogenation by mixing different molecular sieves in the support. *Fuel Process. Technol.* **2010**, *91*, 1655–1661. [[CrossRef](#)]
8. Pinilla, J.L.; Garcia, A.B.; Philippot, K.; Lara, P.; Garcia-Suarez, E.J.; Millan, M. Carbon-supported Pd nanoparticles as catalysts for anthracene hydrogenation. *Fuel* **2014**, *116*, 729–735. [[CrossRef](#)]
9. Yang, Y.; Li, J.; Lv, G.; Zhang, L. Novel method to synthesize Ni₂P/SBA-15 adsorbents for the adsorptive desulfurization of model diesel fuel. *J. Alloys Compd.* **2018**, *745*, 467–476. [[CrossRef](#)]
10. Song, H.; Wang, J.; Wang, Z.D.; Song, H.L.; Li, F.; Jin, Z.S. Effect of titanium content on dibenzothiophene HDS performance over Ni₂P/Ti-MCM-41 catalyst. *J. Catal.* **2014**, *311*, 257–265. [[CrossRef](#)]
11. Fang, M.; Tang, W.; Yu, C.; Xia, L.; Xia, Z.; Wang, Q.; Luo, Z. Performance of Ni-rich bimetallic phosphides on simultaneous quinoline hydrodenitrogenation and dibenzothiophene hydrodesulfurization. *Fuel Process. Technol.* **2015**, *129*, 236–244. [[CrossRef](#)]
12. Tian, S.; Li, X.; Wang, A.; Chen, y.; Li, H.; Hu, Y. Hydrodenitrogenation of quinoline and decahydroquinoline over a surface nickel phosphosulfide phase. *Catal. Lett.* **2018**, *148*, 1579–1588. [[CrossRef](#)]
13. Yun, G.; Guan, Q.; Li, W. Nondestructive construction of Lewis acid sites on the surface of supported nickel phosphide catalysts by atomic-layer deposition. *J. Catal.* **2018**, *361*, 12–22. [[CrossRef](#)]
14. Hu, D.; Duan, A.; Xu, C.; Zheng, P.; Li, Y.; Xiao, C.; Liu, C.; Meng, Q.; Li, H. Ni₂P promotes the hydrogenation activity of naphthalene on wrinkled silica nanoparticles with tunable hierarchical pore sizes in a large range. *NanoScale* **2019**, *11*, 15519–15529. [[CrossRef](#)] [[PubMed](#)]
15. Oyama, S.T.; Lee, Y.K. The active site of nickel phosphide catalysts for the hydrodesulfurization of 4,6-DMDBT. *J. Catal.* **2008**, *258*, 393–400. [[CrossRef](#)]
16. Vargas-Villagrán, H.; Ramírez-Suárez, D.; Ramírez-Muñoz, G.; Calzada, L.A.; González-García, G.; Klimova, T.E. Tuning of activity and selectivity of Ni/(Al)SBA-15 catalysts in naphthalene hydrogenation. *Catal. Today* **2021**, *360*, 27–37. [[CrossRef](#)]
17. Tan, Q.; Cao, Y.; Li, J. Prepared multifunctional catalyst Ni₂P/Zr-SBA-15 and catalyzed Jatropa Oil to produce bio-aviation fuel. *Renew. Energy* **2020**, *150*, 370–381. [[CrossRef](#)]
18. Jing, J.Y.; Wang, J.Z.; Liu, D.C.; Qie, Z.Q.; Bai, H.C.; Li, W.Y. Naphthalene hydrogenation saturation over Ni₂P/Al₂O₃ catalysts synthesized by thermal decomposition of hypophosphite. *ACS Omega* **2020**, *5*, 31423–31431. [[CrossRef](#)]
19. Jing, J.Y.; Yang, Z.F.; Wang, J.Z.; Liu, D.C.; Feng, J.; Li, W.Y. Effect of preparation methods on the structure and naphthalene hydrogenation performance of Ni₂P/SiO₂ catalyst. *J. Fuel Chem. Technol.* **2020**, *48*, 842–851. [[CrossRef](#)]
20. Hédoire, C.E.; Louis, C.; Davidson, A.; Breyse, M.; Maugé, F.; Vrinat, M.; Hédoire, C.E.; Louis, C.; Davidson, A.; Breyse, M. Support effect in hydrotreating catalysts: Hydrogenation properties of molybdenum sulfide supported on β -zeolites of various acidities. *J. Catal.* **2003**, *220*, 433–441. [[CrossRef](#)]
21. Lan, X.; Hensen, E.J.M.; Weber, T. Silica-supported Ni₂P: Effect of preparation conditions on structure and catalytic performance in thiophene hydrodesulfurization (HDS). *Catal. Today* **2017**, *292*, 121–132. [[CrossRef](#)]
22. Oyama, S.T.; Gott, T.; Zhao, H.; Lee, Y.-K. Transition metal phosphide hydroprocessing catalysts: A review. *Catal. Today* **2009**, *143*, 94–107. [[CrossRef](#)]
23. Guan, Q.; Li, W. A novel synthetic approach to synthesizing bulk and supported metal phosphides. *J. Catal.* **2010**, *271*, 413–415. [[CrossRef](#)]
24. Wu, H.; Ni, Y.; Wang, M.; Lu, D. Shape-controlled synthesis and performance comparison of Ni₂P nanostructures. *CrystEngComm* **2016**, *18*, 5155–5163. [[CrossRef](#)]
25. Wang, J.; Wang, Y.; Chen, G.; He, Z. Highly loaded and dispersed Ni₂P/Al₂O₃ catalyst with high selectivity for hydrogenation of acetophenone. *Catalysts* **2018**, *8*, 309. [[CrossRef](#)]

26. Chu, S.; Li, X.; Zhou, X.R.; Prins, R.; Waqas, Q.; Wang, A.J.; Sheng, Q.; Hao, Q.L. Preparation of Ni₂P supported on Al₂O₃ and B₂O₃ mixed oxides by yemperature-programmed reduction of phosphate precursors withLow P/Ni ratios. *Top. Catal.* **2020**, *63*, 1379–1387. [[CrossRef](#)]
27. Bussell, M.E.; Miles, C.E.; Carlson, T.R.; Morgan, B.J.; Topalian, P.J.; Schare, J.R. Hydrodesulfurization properties of nickel phosphide on borontreated alumina supports. *ChemCatChem* **2020**, *12*, 4939–4950.
28. Dang, Y.; Liu, Y.B.; Feng, X.; Chen, X.B.; Yang, C.H. Effect of dispersion on the adsorption of polycyclic aromatic hydrocarbons over the γ -Al₂O₃ (110) surface. *Appl. Surf. Sci.* **2019**, *486*, 137–143. [[CrossRef](#)]